# A Heterocyclic Inhibitor of the Rev−RRE Complex Binds to RRE as a Dimer†

Ke Li,‡ Tina M. Davis,‡ Christian Bailly,§ Arvind Kumar,‡ David W. Boykin,‡ and W. David Wilson*,‡

*Department of Chemistry and Laboratory for Chemical and Biological Sciences, Georgia State University, Atlanta, Georgia 30303, and INSERM U-524 et Laboratoire de Pharmacologie Antitumorale du Centre Oscar Lambret, IRCL, Place de Verdun, 59045 Lille, France*

*Received October 5, 2000; Revised Manuscript Received December 1, 2000*

ABSTRACT: As part of a search for organic compounds that selectively target RNA, we found that specific diphenylfuran derivatives, which are related to compounds that bind to the DNA minor groove, bind very strongly to RNA in a manner very sensitive to the structure of the compounds. In extended development of the diphenylfuran series, we found that a tetracationic heterocycle containing a phenyl-furan-benzimidazole unfused aromatic system, DB340, exhibits pronounced selectivity for the RRE RNA stem-loop from HIV-1. We report here RNA footprinting, spectroscopic analysis, affinity determinations, and initial NMR structural results of the complex. The results indicate that DB340 binds to RRE in a highly structured and cooperative complex at a 2:1 DB340 to RRE ratio. Overlap in the NMR spectra prevents detailed description of binding interactions at this time, but we are able to place DB340 in the RNA minor groove. Additionally, footprinting results and studies with mutant RRE sequences indicate that the internal loop of RRE is required for specific binding of DB340 as with the Rev protein. These results provide exciting new ideas for rational drug design with RNA as is now common with DNA and proteins.

Since some of the most devastating human diseases are caused by RNA viruses, such as HIV and hemmoragic fever viruses such as Dengue, West Nile, and Ebola (*1*), RNA is an attractive therapeutic target in drug design (*2*−*5*). Despite the potential advantages of directly targeting the RNA of these viruses, few drugs are known that have RNA as their bioreceptor. Rational design of drugs that target RNA is in the beginning stages (*2*, *3*, *6*−*10*) and has been largely focused around the aminoglycoside class of compounds (*2*, *10*, *11*).

The base and backbone similarities of DNA and RNA suggest that compounds that target DNA may provide initial models for the development of compounds that target RNA duplexes. Intercalators that interact with both DNA and RNA (reviewed in ref *12*) are well-known, but methods to increase the selectivity of intercalating systems for RNA structures have not yet emerged. Efforts to target the minor groove of DNA have progressed markedly within the past decade and currently are the model for rational design of compounds to selectively interact with nucleic acids (*13*−*21*). Although the chemical similarities between DNA and RNA are obvious, the low-energy duplex structures of these molecules differ significantly, particularly in groove geometry (*22*). Additionally, the unique structural folds present in RNA but not DNA offer the possibility of much higher recognition specificity by small molecules than that for DNA (*23*). Structured sites in RNA should be able to be targeted with the same specificity with small molecules as structured binding regions of proteins.

As part of a search for organic compounds that selectively target RNA, we found that specific diphenylfuran derivatives, which are related to compounds that bind to the DNA minor groove (*24*, *25*), bind very strongly to RNA in a manner very sensitive to the structure of the compounds (*6*, *26*−*29*). In extended development of the diphenylfuran series, we found that DB340 (Figure 1) exhibited pronounced affinity and modest selectivity for the RRE RNA stem-loop from HIV-1 (ref *29* and unpublished results). To continue development of the diphenylfuran series to enhance both affinity and selectivity of these small aromatic cations for RNA, and to use this example to develop new RNA directed compounds, we sought to establish the details of the DB340−RRE complex. As a part of this process, we report here RNA footprinting, spectroscopic analysis, affinity determinations, and initial NMR structural results of the complex. The results indicate that DB340 binds to RRE in a highly structured and cooperative complex at a 2:1 DB340 to RRE ratio. Overlap in the NMR spectra prevents detailed description of binding interactions at this time, but we are able to place DB340 in the RNA minor groove. Additionally, footprinting results and studies with mutant RRE sequences indicate that the internal loop of RRE is required for specific binding of DB340 as with the Rev protein. These results provide exciting new ideas for rational drug design with RNA as is now common with DNA and proteins.

## METHODS

*Materials.* The synthesis of DB340 will be reported elsewhere. Oligoribonucleotides except RRE hp 2 (Figure 1) were purchased from Cruachem (Dulles, VA) and were

† This work was supported by NIH research grants (to W.D.W and R.R.T) and from the INSERM, ARC, and the Ligue Nationale Frangaise Contre le Cancer (Comité du Nord) (to C.B). Instrumentation was purchased through funds from the Georgia Research Alliance.

* To whom correspondence should be addressed. Phone: 404-651-3903. Fax: 404-651-2751. E-mail: chewdw@panther.gsu.edu.

‡ Georgia State University.

§ INSERM U-524 et Laboratoire de Pharmacologie Antitumorale du Centre Oscar Lambret, IRCL.

10.1021/bi002338b CCC: $20.00 
Published on Web 01/11/2001

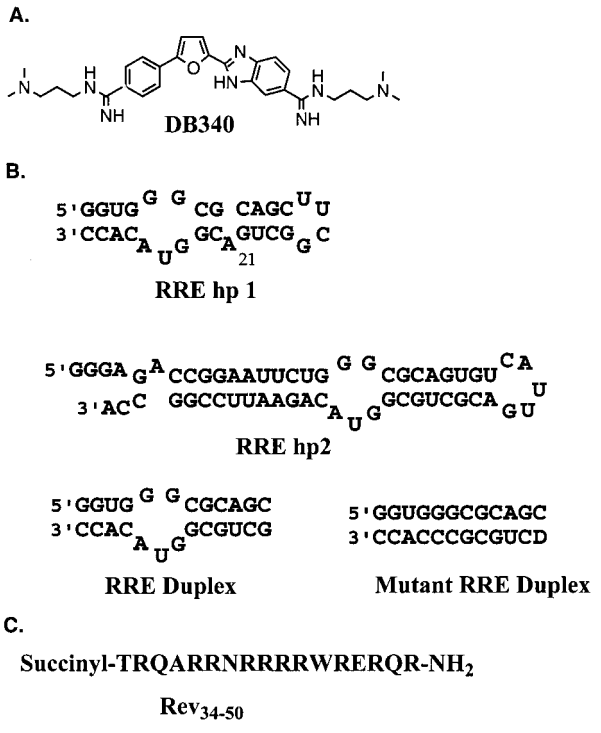


FIGURE 1: (A) Structure of RRE-binding compound DB340. (B) The sequences and secondary structures of the RRE duplex and hairpin models used in this study. The numbering of the nucleotides is shown. Note the different numbering for RRE hp 2. (C) The sequence of the $Rev_{34-50}$ peptide.

prepared on an ABI 380B synthesizer using standard RNA assembly protocols via phosphoramidite method and purified by ion exchange HPLC. RRE hp 2 was transcribed as a runoff product as described in the footprinting section below. 5′-Biotinylated RRE RNA for SPR experiments was obtained from Cruachem. RRE was further purified by electrophoresis on a 15% polyacrylamide denaturing gel. Full-length biotin-RRE was excised from the gel and electroeluted (Schleicher and Scheull) into TBE. Biotin-RRE was exchanged into distilled deionized water and concentrated with Centricon-3 (Amicon). All the RRE models were annealed by heating to 90 °C before use. The $Rev_{34-50}$ peptide was prepared as previously described (*30*, *31*). The termini modifications have been shown to increase alpha-helicity and binding to RRE relative to peptides with native termini (*30*−*32*).

Streptavidin functionalized Biacore sensorchips (SA-chips) and HBS buffer [10 mM HEPES, pH 7.4, 150 mM NaCl, 3 mM EDTA, 0.005% (v/v) Surfactant P20, filtered and degassed] were obtained from Biacore Inc. Low stringency binding buffer (LBS) (HBS plus 150 mM NaCl) and medium stringency binding buffer (MBS) (HBS plus 350 mM NaCl) were made from HBS buffer purchased from BIAcore. 300 mM $Na_2SO_4$ for regeneration was filtered through a 0.2 $\mu$m filter and degassed for 30 min prior to use.

*RNA Footprinting.* RRE hp 2 was transcribed as a runoff product from a previously described plasmid according to a published procedure (*33*). The RNA was transcribed as a runoff product of 57 nucleotides from the T3 RNA polymerase promoter. Transcription reaction was performed in buffer containing 40 mM Tris-HCl, pH 7.4, 25 mM NaCl, 16 mM MgCl2, 10 mM DTT, and 1 mM M NTPs. The reaction was initiated by addition of 10 $\mu$g of linearized plasmid DNA template and 40 units of T3 RNA polymerase and incubated for 2 h at 37 °C. Nucleic acids were then fractionated on a 10% (w/v) polyacrylamide gel containing 8 M urea in TBE buffer (89 mM Tris base, 89 mM boric acid, and 10 mM EDTA). After electrophoresis, the RNA was eluted in water for 18 h at 4 °C and precipitated with ethanol. The RNA was 3′ end-labeled with $^{32}P$ cytidine biphosphate and T4 RNA ligase and then repurified from a 10% denaturing acrylamide gel. RNA solutions were prepared with doubly distilled sterile water to prevent nuclease contamination. Tubes and tips were treated with diethylpyrocarbonate (DEPC from Sigma).

RRE hp 1 was purchased from Cruachem and end-labeled using [$\gamma^{32}P$]ATP and T4 polynucleotide kinase under standard conditions. The concentration of radiolabeled RNAs were calculated from the specific activity of $^{32}P$ incorporation.

The procedure for footprinting experiments was adapted from published protocols (*34*, *35*). Briefly, the labeled RNA hairpin was equilibrated with buffered solutions at the desired drug concentration and digestion was initiated by addition of a solution of each RNase. After 1 min incubation at room temperature, reactions were stopped by freeze-drying, and samples were lyophilized. The RNA in each tube was resuspended in 5 $\mu$L of formamide-TBE loading buffer, denatured at 90 °C for 4 min, and then chilled on ice for 5 min prior to loading onto a 0.3-mm-thick 10% polyacrylamide gel containing 8 M urea and TBE buffer (89 mM Tris base, 89 mM boric acid, 2.5 mM EDTA, pH 8.3). After electrophoresis, the gel was soaked in 10% acetic acid for 10 min, transferred to Whatman 3MM paper, dried under vacuum at 80 °C, and analyzed with a phosphorimager (Molecular Dynamics). A sequencing standard was generated by treatment of the RNA with diethylpyrocarbonate followed by aniline-induced cleavage at the modified bases (A track lane).

*UV−Vis Spectroscopy.* UV−Vis scans and thermal denaturation experiments were collected on a Cary 4 spectrophotometer interfaced to a Dell/486 microcomputer. The absorbance spectra of DB340 were recorded in a 1-cm cell in 10 mM sodium phosphate buffer (pH 7.0) containing 0.1 M NaCl and 1 mM EDTA. Melting temperatures ($T_m$) of the RRE RNA in the absence and presence of DB340 were determined in the same buffer.

*Fluorescence Spectroscopy.* Fluorescence measurements were conducted as described previously (*29*). Briefly, titration was conducted in 4 × 4 mm quartz cells coated with Sigmacoat (Sigma). DB340 was diluted in 250 $\mu$L of 10 mM sodium phosphate buffer (pH 7) containing 1 mM EDTA and 0.1 M NaCl to give the desired final concentration. After each addition of RRE, the sample was excited at 356 nm, and the fluorescence was monitored at 456 nm. The excitation and emission slit widths were 1−2 and 4 nm, respectively. Integration times were 1 s, and each data point was an average of three measurements. Titrations were continued until no further change in fluorescence was observed upon addition of RRE. Binding constants ($K_A$) were calculated by Scatchard analysis.

*Surface Plasmon Resonance.* RRE RNA was immobilized on streptavidin coated sensorchips as described (*20*, *21*). 290 RU of biotin-RRE was immobilized on flowcell 2 and 227 RU biotin-RRE was immobilized on flowcell 3. DB340 samples were prepared in the appropriate buffer by serial

dilutions from a 100 $\mu$M stock solution. Binding data was collected using an automated method. Buffer was injected in the first two cycles to establish a stable baseline. DB340 was subsequently injected for 5 (high concentration) or 10 (low concentration) min using the KINJECT command and a flowrate of 10 $\mu$L/min. Concentrations of DB340 ranged from 25 nM to 10 $\mu$M. Samples were injected from 7-mm sterile plastic vials with pierceable caps at increasing concentrations of DB340 to minimize carry over. One injection of 300 mM $Na_2SO_4$ and two injections of LSB buffer were used between concentrations to regenerate the RNA surface.

The RRE surface was periodically monitored for degradation using the Rev peptide. 10 $\mu$M Rev was injected over the control and RNA flowcells for 5 min at a flowrate of 10 $\mu$M/min at the beginning and end of each DB340 experiment. The maximal RU responses (steady-state RU, $R_{eq}$) were compared to assess the integrity of the RNA surface. There was no significant change in the sensorchip surface over the course of the experiments.

The theoretical response of one equivalent of DB340 bound was calculated as described (*21*). Binding constants were determined by fitting the steady-state response versus concentration binding curve using a four-site binding model where the binding constants for two specific binding sites are treated as equal and the binding constants for two nonspecific binding sites are treated as equal. Fitting the data with separate binding constants for the specific binding sites did not significantly increase the quality of the fit.

*Proton NMR Spectroscopy.* RRE samples (typically about 3 mg) were dissolved in 600 $\mu$L of 10 mM sodium phosphate buffer containing 0.1 M NaCl and 5 $\times$ 10−5 M EDTA, pH 6.5. A stock solution of DB340 was added to the RNA solution to give desirable molar ratios of drug to RNA. After each addition, the RNA sample was dried, and the volume was brought back to 600 $\mu$L in either 90% $H_2O$/10% $D_2O$ or $D_2O$ for exchangeable and nonexchangeable proton spectra, respectively.

All proton NMR spectra were acquired on a Varian Unity Plus 600 MHz spectrometer. Data were processed with Vnmr 5.3 software or FELIX 2.30 (Biosym Tech., San Diego, CA). One-dimensional exchangeable proton spectra of RRE were recorded at 5 °C with blocks of 4096 complex points and sweep width of 12 000 Hz. Binomial pulse sequence was used for water suppression. $H_2O$ NOESY spectra were acquired at 5 °C in phase sensitive mode using 100 and 250 ms mixing time. The WATERGATE pulse sequence (*36*) was used for water suppression.

Two-dimensional experiments focusing on the nonexchangeable protons were obtained in $D_2O$ with a spectral width of 600 Hz in both dimensions with 2048 complex data points in the t2 dimension and 512 points in the t1 dimension and a mixing time of 250 ms (for NOESY experiments).

## RESULTS

*NMR.* The 30mer RRE hairpin 1 has been used in NMR studies of the Rev-RRE complex (*37*). It contains a UUCG tetraloop that gives characteristic resonance peaks for exchangeable and nonexchangeable protons. We have also found that the proton resonances of the RRE hairpin 1−DB340 complex are sharper than those of the RRE duplex−DB340 complex, probably because DB340 binds more strongly to the hairpin than to the duplex (below), and there is less effect of end fraying in the hairpin. Therefore, all the NMR spectroscopic studies reported here are for the RRE hairpin 1.

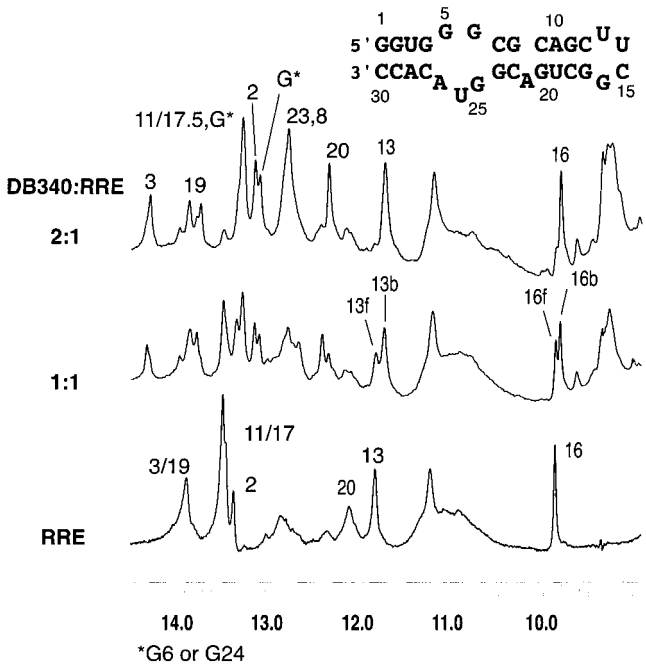


FIGURE 2: One-dimensional imino proton spectra of the RRE hairpin titrated with DB340. The imino resonances of U13 and G16 for both the free (f) and DB340 bound (b) hairpin are labeled and demonstrate the complex is in slow exchange with unbound RRE. The spectra were recorded at 5 °C in 10 mM sodium phosphate buffer (pH 6.5) containing 0.1 M NaCl and 5 $\times$ $10^{-5}$ M EDTA in 90% $H_2O$/10% $D_2O$.

*One-Dimensional Imino Proton Spectra of DB340-RRE Complex.* Formation of the DB340−RRE complex was monitored by following the imino proton spectra of RRE hp 1 titrated with DB340. The imino protons of the free RRE hp 1 have been assigned in previous structural studies (*37*, *38*), and our spectra for the free RNA are consistent with the published results (Figure 2). Some of the imino resonances of RRE complexed with DB340 have been assigned based on 1D NOE difference spectra, DB340 titration experiments, and 2D NOESY experiments. The characteristic resonance positions of the imino protons of U13 and G16 in the complex are shifted upfield of the other imino protons (characteristic of UUCG tetraloops) and shift only slightly upon complex formation during titration of RRE with DB340. DB340 binding is most clearly demonstrated by following the small changes of these imino proton resonances, which are in a relatively uncluttered region (Figure 2). In the presence of a 1:1 molar ratio of DB340, two equal sets of imino proton resonances were observed, one for the free RRE and a new set of signals for DB340-bound RRE. At a 2:1 molar ratio of DB340, only the peaks for the bound form were observed. Only one new set of resonances for the bound RRE at both 1:1 and 2:1 molar ratios of DB340 indicates that only the 2:1 complex forms. The 2:1 complex and free RNA at a 1:1 molar ratio strongly suggests a highly cooperative binding mode for the DB340 dimer.

The most dramatic imino proton spectral change of the RRE hairpin upon complex formation with DB340 occurred

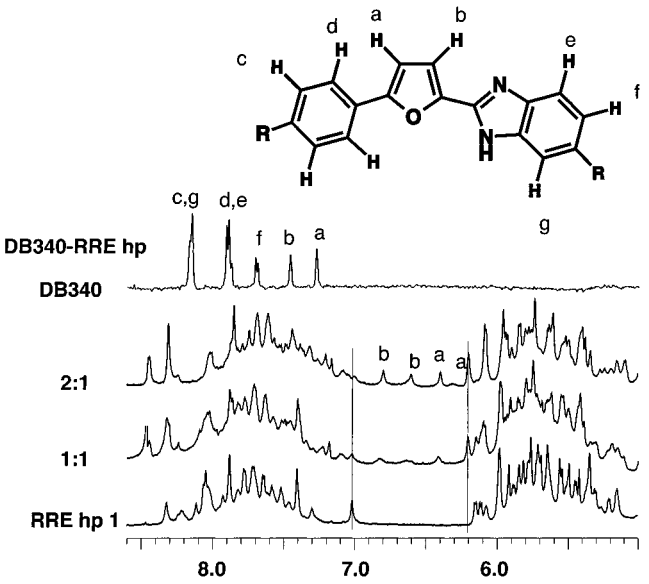


FIGURE 3: One-dimensional spectra of the nonexhangeable aromatic and H5/H1′ protons of the RRE hairpin and DB340. The molar ratios of DB340 to the RRE are indicated. The spectra were recorded in 10 mM phosphate buffer (pH 7.0) in $D_2O$ containing $1 \times 10^{-5}$ M EDTA and 0.1 M NaCl at 35 °C. The furan protons (a and b) of DB340 are labeled and show two new peaks for both furan protons even at the 1:1 DB340/RRE ratio.

in the 12−13.4 ppm region (Figure 2). For free RRE, only very broad peaks were observed in much of this region. Previous studies have shown that these broad peaks correspond to the nucleotides in the internal loop and the C−G and G−C base pairs in the upper stem immediately adjacent to the internal loop. The broad lines are a result of conformational flexibility in this region (*37*, *38*). Upon complex formation with DB340, additional resonance peaks appeared in this region, and significant peak sharpening was observed, as was also observed upon Rev binding (*37*, *38*). These changes indicate that DB340 binding significantly stabilizes base-pairing in the internal loop region since sharp imino proton resonances are normally associated with hydrogen bonded bases in slow exchange with water.

*Nonexchangeable Proton Spectra of DB340/RRE Complex.* The aromatic proton spectra of the RRE−DB340 complex have sharp resonance peaks in the aromatic and the H5/H1′ regions that again support formation of a strong, specific complex (Figure 3). Upon binding to DB340, significant changes in the dispersion of the chemical shifts in both the aromatic and the H5/H1′ regions were observed. For example, RNA protons in the aromatic region shifted generally downfield from ∼7.0−8.3 to 7.1−8.5 ppm. There are also significant changes in the spectra of DB340 protons. Upon titration of the RRE hairpin with DB340, two new sets of resonances are observed for each of the DB340 protons at both 1:1 and 2:1 ratios of DB340 to RRE (Figure 3). This is most clearly demonstrated by the furan protons (labeled a and b in Figure 3). Doubling of the DB340 proton resonances even at the 1:1 ratio is consistent with formation of a specific and cooperative 2:1 complex with the two bound DB340 molecules in different environments with slow exchange.

The chemical shifts of DB340 aromatic protons in the free and RRE-bound forms were assigned based on temperature-dependent 1D spectra, 2D COSY, and NOESY spectra (Table 1). DB340 has four pairs of adjacent aromatic protons (one furan, one benzimidazole, and two phenyl) that are expected to give only three individual cross-peaks (one furan, one benzimidazole, and one phenyl) in the COSY spectrum of unbound DB340 due to rapid rotation of the phenyl ring. As shown in Figure 4, at the 2:1 ratio, two new sets of cross-peaks are observed for each of the furan and benzimidazole protons of DB340 and none of the free DB340 cross-peaks are observed. Additionally, upon binding to RRE, rotation of the phenyl ring is reduced so that the two sets of adjacent phenyl protons give separate resonances although only 3 of 4 possible sets of phenyl cross-peaks are resolved. Large upfield shifts were observed for all the aromatic protons of DB340 suggesting aromatic ring stacking in the complex. The aromatic protons of DB340 that are closer to the center of the molecule, including the furan protons a and b, the phenyl proton d, and the benzimidazole proton e, showed larger shifts upon binding to the RRE (Table 1).

Only one set of H5−H6 cross-peaks is observed for RRE in COSY spectra (data not shown). These results are

Table 1: Chemical Shifts of the Aromatic Protons of DB340

| | aromatic protons of DB340[a,b] | | | | | | |
|---|---|---|---|---|---|---|---|
| | furan | | phenyl | | benzimidazole | | |
| | a | b | c | d | e | f | g |
| free DB340 | 7.28 | 7.45 | 8.09 | 7.86 | 7.83 | 7.67 | 8.06 |
| DB340 | 6.40 (0.88)[c] | 6.81 (0.64) | 7.84 (0.25) | 7.49 (0.37) | 7.09 (0.74) | 7.46 (0.21) | NA[d] |
| + RRE hp | 6.08 (1.20) | 6.60 (0.21) | 7.70 (0.39) 7.52 (0.57) | 7.38 (0.48) 7.34 (0.52) | 7.01 (0.82) | 7.48 (0.19) | |

[a] Labeling of the protons is shown in Figure 3. [b] Furan, benzimidazole, and phenyl proton pairs are next to each other. However, it is not clear which pairs of furan, benzimidazole, and phenyl protons are for the same molecule. [c] Change in chemical shift is shown in parentheses. [d] Not assigned.

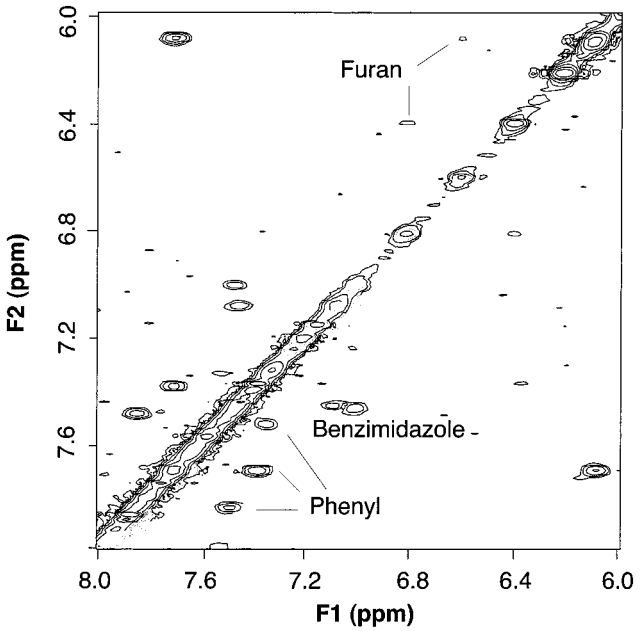


FIGURE 4: The aromatic region of the COSY spectrum of the 2:1 DB340/RRE complex. The cross-peaks for the aromatic protons of DB340 are labeled. Notice that two sets of cross-peaks are observed for each pair of aromatic protons.

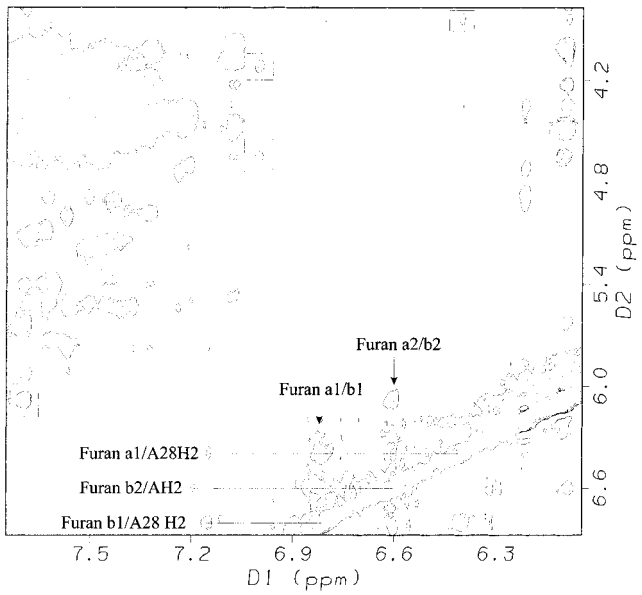


FIGURE 5: The aromatic and H5/H1′ region of the NOESY spectrum of the 2:1 DB340/RRE complex. Cross-peaks between A28 H2 and furan protons a and b of the same molecule are indicated. A cross-peak between the furan b proton of the second bound DB340 and an unassigned AH2 proton is marked. Cross-peaks between benzimidazole and furan protons to unassigned H1′ protons are boxed. These cross-peaks place the DB340 dimer in the RNA minor groove near the G−A base pair end of the internal bulge.

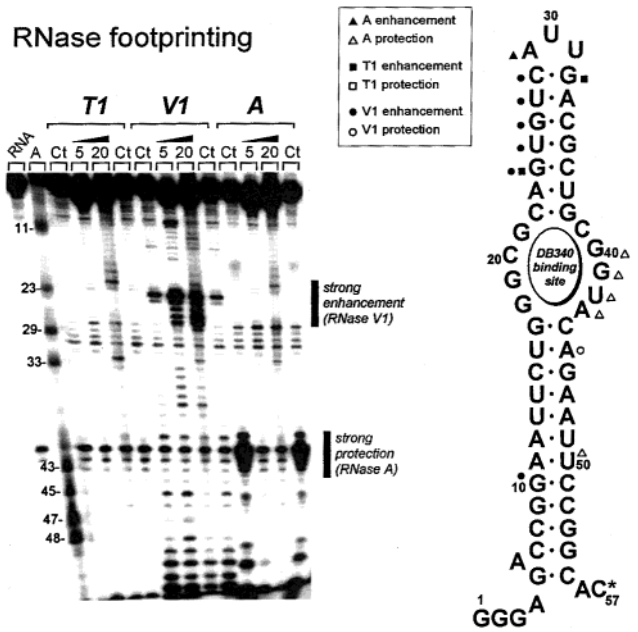


FIGURE 6: RNase V1, T1, and A footprinting of RRE hairpin at increasing concentrations of DB340. The strong RNase V1 cleavage enhancement in the upper stem and RNase A cleavage protection in the bulge are indicated on the gel. The enhancement/protection pattern is indicated by symbols described in the box.

consistent with a ratio of two compounds to one RNA hairpin model and confirm that the complex is in slow exchange. The COSY spectrum of the DB340/RRE complex at a 1:1 molar ratio showed the same two sets of cross-peaks for DB340 and no free DB340 (data not shown), confirming that a 1:1 complex does not form at any significant concentration. The H5 protons of the C and U bases in the DB340/RRE complex were identified based on the H5 to H6 cross-peaks in the COSY spectrum. There is a 2 ppm dispersion (4.1 to 6.1 ppm) for the H5 protons. This is a significant increase as compared to the dispersion of only 1.0 ppm (5.1−6.1 ppm) in the free RRE and is very similar to the increased dispersion observed upon Rev binding (1.9 ppm) (*38*).

The extended aromatic region of the NOESY spectrum of the 2:1 DB340/RRE complex is shown in Figure 5. As in the COSY spectrum, two sets of cross-peaks were observed for the aromatic protons of DB340 in the NOESY spectrum. In addition, weak cross-peaks resulting from the chemical exchange between the two species of the furan protons were also observed. A strong cross-peak from one furan proton (b) and a weak cross-peak from the other furan proton (a) on the same molecule to the H2 of A28 are observed. The H2 of A28 was assigned through a strong cross-peak to the imino proton of U3 (not shown). The imino proton of U3 is the most downfield resonance in the RRE−DB340 complex and its assignment is very similar in the Rev−RRE complex. A cross-peak between the furan proton b of the second bound DB340 molecule and an unassigned AH2 proton is also observed (Figure 5). The resonance was identified as an AH2 through a strong cross-peak to an unassigned imino proton and its lack of other cross-peaks to the H1′ region. Additionally, we observe cross-peaks between benzimidazole and furan protons to unassigned H1′ protons (Figure 5). These cross-peaks place the drug dimer in the minor groove and orient the furan protons of DB340 toward the bases of RRE.

*RNase Footprinting.* RNase footprinting experiments were performed with both the long and short hairpin models (Figure 1) to probe the binding sites of DB340 on the RRE molecule. The longer RRE hp 2 was used for most footprinting experiments since it provided better defined gel patterns than the shorter hairpin. RRE hp 2 contains the same base sequence as RRE hp 1 except residue A21 of hp 1 is deleted. Deletion of this residue does not significantly affect the RNA structure or binding of the Rev peptide (*33*, *39*). RNase V1, T1, and A were used for RNA cleavage (Figure 6). The most striking results with the double-strand-cleaving RNA nuclease V1 are the cleavage enhancements in the stem near the hairpin loop (G24−C28), indicating an improved A-form helical stacking in this region of the drug complex. It is clear that binding of DB340 does not cause any decrease in the access of the enzyme to the upper stem region and indicates that this region is not a drug binding site. There is also protection from V1 cleavage at A45. The decrease in cleavage observed at A45 (A28 of the RRE hp 1) is consistent with the NMR results described above that indicate the drug dimer binds at or near this site on the RNA.

Very significant changes in RNase A cleavage of the RRE segment occur on complex formation (Figure 6). RNase A cleaves the internal loop region (G40−A43) very strongly in the free RNA, but the cleavage is almost completely inhibited on complex formation with DB340. Protection of the internal bulge from RNase A cleavage reflects improved stacking and suggests binding of DB340 to this region. There is some protection of cleavage at U50 and an enhancement of cleavage by RNase A in the hairpin loop at A29. RNase T1 cleavage is not markedly affected by complex formation, although there is a slight enhancement of cleavage by T1 at G24 and G32 in the upper hairpin stem region in the DB340 complex.

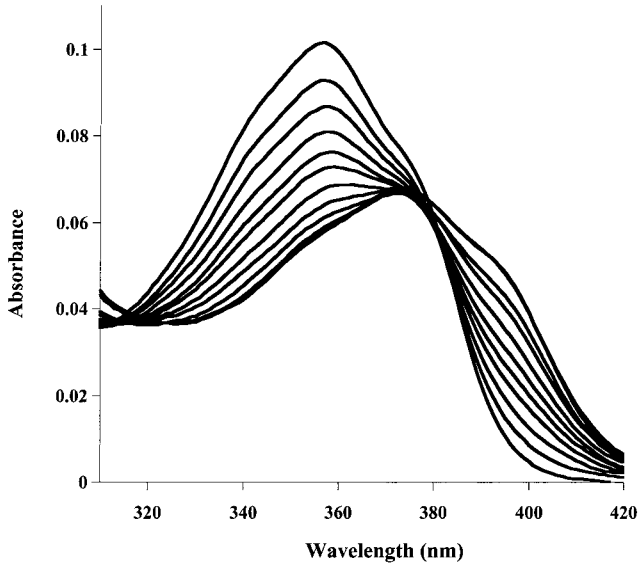


FIGURE 7: Spectroscopic titration of DB340 with RRE hairpin. Titration was conducted at 25 °C in a 1-cm cell in 10 mM sodium phosphate (pH 7.0) containing 0.3 M NaCl and 1 mM EDTA and was monitored at 356 nm. An isosbestic point near 380 nm is present until a ratio of 2:1 and is lost upon further addition of the RRE hairpin. The concentration of DB340 was 2.4 $\mu$M. The concentrations of the RRE hairpin were 0.04, 0.21, 0.37, 0.53, 0.69, 0.84, 1.24, 1.64, 2.24, 3.03, and 3.42 $\mu$M from the top to the bottom curves.

Although not of as high a quality, RNase footprinting of RRE hp 1 gave results in agreement with those from the longer sequence. Enhancement of RNase V1 cleavage by DB340 at the upper stem region and protection of RNase A cleavage by DB340 in the internal loop region were observed (data not shown).

*UV and Fluorescence Spectroscopies.* DB340 has absorption bands in the 300 to 400 nm spectral area that are separated from the RNA absorption region. Addition of RRE results in a hypochromic effect along with a shift of the absorption maximum to longer wavelength (Figure 7). An isosbestic point near 380 nm is present at stoichiometric ratios up to 2:1 DB340 to RRE indicating that a single mode of strong binding dominates throughout this range and is consistent with NMR results that indicate preferential formation of the specific 2:1 complex. At DB340 to RRE ratios greater than 2:1, the isobestic point is lost suggesting a secondary binding mode at higher concentrations. This secondary binding mode is most likely nonspecific binding of the tetracation to RRE and is observed in quantitative SPR and fluorescence experiments (below) as well as line broadening in NMR experiments at ratios greater than 2:1.

UV absorbance melting experiments showed a concentration-dependent rise of the melting temperature $T_m$ of RRE duplex upon addition of DB340 (data not shown). At a 2:1 ratio of DB340 to RRE, the $T_m$ increased 6 °C. The $T_m$ of the mutant RRE duplex (Figure 1) increased only 2 °C, however, at this ratio. Such a difference in the increase in $T_m$ indicates a significant difference in the stability of the two complexes upon binding of DB340 and a requirement for the RRE internal loop for the strong 2:1 complex.

Excitation of DB340 in its absorption region results in a strong fluorescence emission spectrum with a maximum near 460 nm. Upon titration with RRE, there is a concentration-dependent and saturable decrease of the fluorescence intensity of DB340. Scatchard plots of fluorescence binding data (Figure 8) reveal significant differences in the way that DB340 binds to RRE and the mutant sequence. DB340 binds very strongly to RRE with a stoichiometric ratio of two specific DB340 binding sites per RRE. Since the binding constant for each site cannot be resolved, we report an observed $K_A$ of $1.4 \times 10^8$ obtained by fitting the first approximately linear region of the Scatchard plot. Previous results have shown that DB340 binds to RRE hp 1 with the same 2:1 stoichiometry and similar binding constant (*29*). At ratios above 2:1 DB340 to RRE, nonspecific binding is observed between the tetracation and RRE. DB340 binds to the mutant RRE sequence with a 5-fold lower binding constant ($K_A$ of $2.5 \times 10^7$) and a stoichiometric ratio approaching 3 DB340 molecules per RRE. The approximate linearity of the Scatchard plot suggests a dominant binding mode that is comparable in affinity to the nonspecific binding seen with the RRE duplex sequence at higher DB340 to RRE ratios (Figure 8).

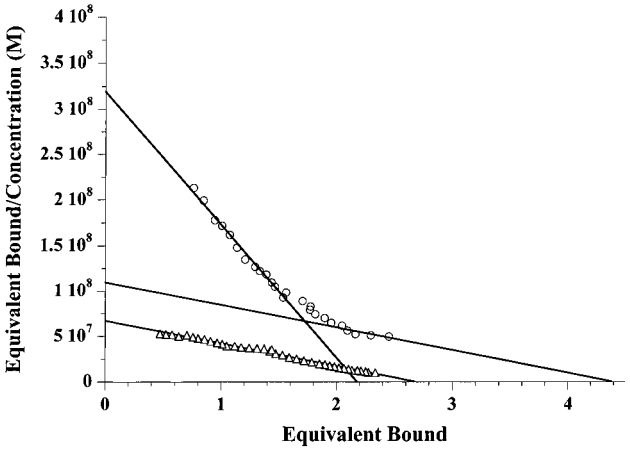


FIGURE 8: Scatchard plots of fluorescence titration of DB340 with the RRE based duplex (circles) and the mutant duplex sequence (triangles). The data indicate that two DB340 molecules bind specifically to RRE and two additional DB340 molecules bind to RRE nonspecifically. Fluorescence binding studies were performed in 10 mM sodium phosphate buffer, pH 7.0, 0.1 M NaCl and 1 mM EDTA. A solution of DB340 (10−50 nM, 250 $\mu$L) in a 4 × 4 mm quartz cell was excited at 356 nm, and the fluorescence intensity was recorded at 455 nm as a function of RRE concentration.

*Surface Plasmon Resonance.* RRE hp 1 containing a biotin moiety attached to the 5′ terminus was immobilized on two cells of a four-cell streptavidin coated sensorchip. One cell of this sensorchip was left as a blank reference cell. Sensorgrams (instrument response versus time) for flow of DB340 concentrations from 25 nM to 10 $\mu$M across the flow cells are shown in Figure 9, panel A. A steady-state response plateau ($R_{eq}$) was achieved at each concentration and was averaged over at least 200 s to yield an $R_{eq}$ value for each concentration. Even at the lowest concentrations of DB340, steady-state response was achieved in under one minute of flow. A Scatchard plot of the steady-state binding data (Figure 9, panel B) confirms the NMR and fluorescence results that indicate there are two specific DB340 binding sites and two additional nonspecific binding sites on RRE hp 1. To obtain binding constants, a four-site binding model was used to fit plots of $R_{eq}$ versus concentration (Figure 9, panel C). The binding constants for the two specific binding

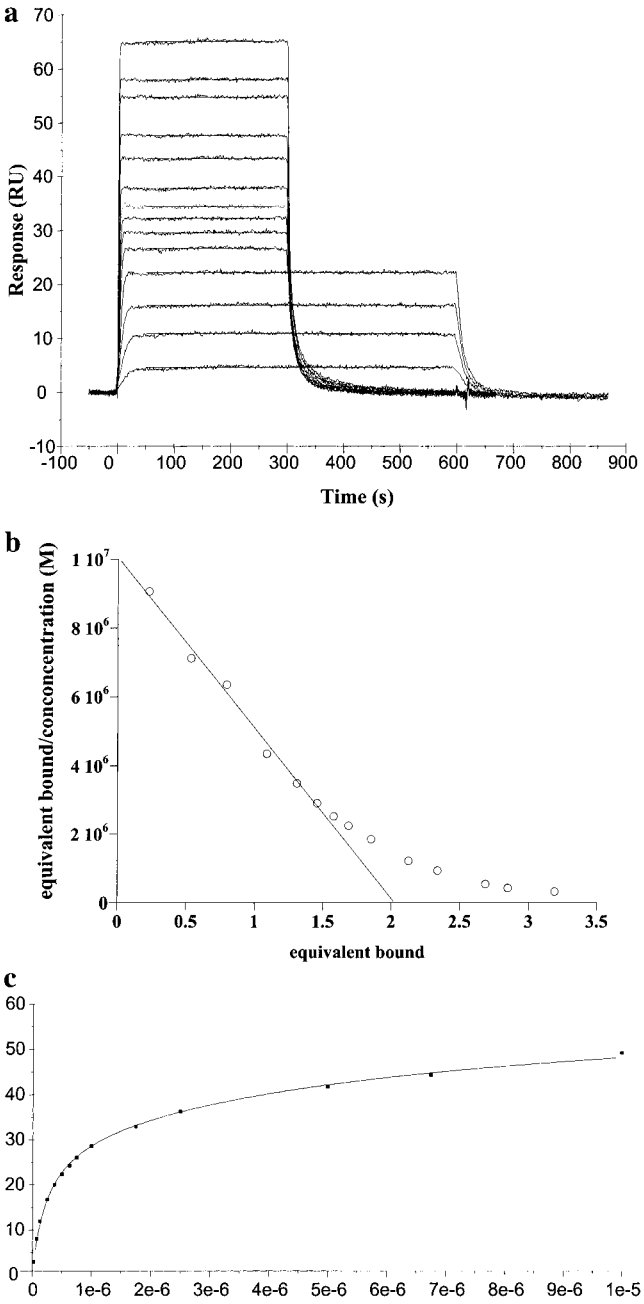


FIGURE 9: Surface plasmon resonance results for binding of DB340 to RRE hairpin 1. (a) Sensorgrams of 25 nM to 10 $\mu$M (bottom to top) DB340 binding to RRE. (b) Scatchard plot of SPR data of DB340 binding to RRE hp 1. As with fluorescence, the results indicate that there are two strong specific DB340 binding sites as well as two nonspecific DB340 binding sites on RRE hp 1. (c) Binding isotherm of the SPR data shown in panel A. The data are shown as points, and the line is the best nonlinear least-squares fit for a four-site binding model where the binding constants for the two specific sites are treated as equal and the binding constants for the two nonspecific sites are treated as equal. Treatment of the data with more complex models, such as four individual sites is not justified by improvement in chi-squared values. SPR binding data were collected in 10 mM HEPES, pH 7.4, 300 mM NaCl, 3 mM EDTA, and 0.005% (v/v) Surfactant P20 at 25 °C.

sites are correlated and difficult to resolve so they are treated as equal. The binding constants for the two nonspecific binding sites are also difficult to resolve and are treated as equal. This gives a model with two classes of sites, each of which can bind two molecules of DB340. At high salt concentration (300 mM $Na^+$), DB340 binds to RRE hp 1 with an observed binding constant of $1.1 \times 10^7$ $M^{-1}$ for the specific binding sites. Binding constants obtained at 100 to 500 mM $Na^+$ indicate that approximately four sodium ions are released per molecule of bound DB340 (Figure 10). This is in complete agreement with the tetracationic charge of DB340. There is excellent agreement between the binding constant obtained through fluorescence (duplex RRE sequence) and those obtained through SPR (RRE hairpin).

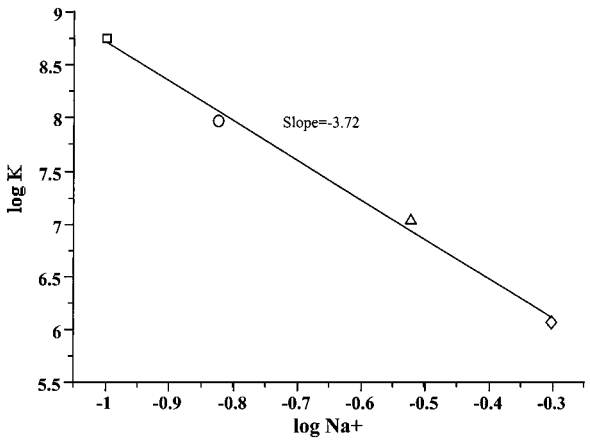


FIGURE 10: Equilibrium constant versus sodium concentration for binding of DB340 to RRE. The square represents the equilibrium constant obtained through fluorescence analysis (duplex RRE) at 100 mM $Na^+$, the circle represents the equilibrium constant obtained through SPR analysis (hairpin RRE) at 150 mM $Na^+$, the triangle represents the equilibrium constant obtained through SPR analysis (hairpin RRE) at 300 mM $Na^+$, and the diamond represents the equilibrium constant obtained through SPR analysis (hairpin RRE) at 500 mM $Na^+$. Linear regression yields a slope of −3.72 indicating approximately four sodium ions are released per molecule of DB340 bound.

NMR results clearly indicate that DB340 binds to RRE in a highly cooperative mode. However, the cooperativity is not observed as convex plots in either the fluorescence or SPR Scatchard plots. The tetracationic charge of DB340 results in nonspecific binding that most likely overlaps with the strong, specific binding and obscures the appearance of cooperative binding.

## DISCUSSION

The RNA−drug index category in the nucleic acid database contains mostly drug (intercalators)−RNA dinucleotide entries and aminoglycoside entries. Rational design of drugs that target RNA has largely focused around aminoglycosides due to their activity as antibacterials (*40*), ribozyme inhibitors (*7*, *41*, *42*), and inhibitors of Rev−RRE and Tat−TAR complex formation (*43*−*45*). While the work with RNA−aminoglycoside complexes is proceeding with promising results, similar studies on other small molecule RNA complexes are needed if RNA is to become a more useful biological receptor for drug design. As part of our effort to develop new model system probes of RNA molecular recognition mechanisms, as well as to develop new paradigms for RNA-directed drug design, we have found that certain diphenylfuran cationic derivatives bind strongly to RNA duplexes. Using inhibition of the Rev−RRE complex as an assay system, we discovered that DB340 is a strong selective inhibitor of complex formation (*29*). The results reported here provide the first structural information on the DB340 complex, and, to our knowledge, this is the first report

of a dimer binding motif in the minor groove of RNA. We also show that the dimer binds specifically near the internal loop of RRE.

The RRE stem-loop of HIV-1 has an asymmetric internal loop that becomes highly structured upon binding of the Rev protein in the major groove (*37*, *38*, *46*, *47*). CD studies suggest that conformational changes occur to the stem-loop upon Rev binding and NMR results clearly demonstrate that the internal loop becomes more structured with reduced dynamics on complex formation (*37*, *38*). The results presented here suggest that DB340 binds in the minor groove near the internal loop region and also results in a more highly ordered structure with no major conformational rearrangement of the RNA upon complex formation. The rapid association rate of DB340−RRE complex formation observed in SPR experiments suggests that no major refolding conformational changes occur upon DB340 binding. Indeed, imino proton NMR and footprinting results indicate that RRE maintains much of its original structure but that DB340 induces significant hydrogen bonding of the internal loop region.

UV melting experiments and the fluorescence binding assay with the mutant RRE duplex clearly show that the internal loop and the G−G and G−A base-pair mismatches are important for high affinity and specific binding of DB340 to RRE. The RNase footprinting experiments on the RRE−DB340 complex (Figure 6) with both the long and the short RRE stem-loop model systems indicate that DB340 binds near the G−A base pair end of the internal loop region and provides strong protection from cleavage of this region by all the enzymes. Reduction in RNase A cleavage at U50 and enhancement of V1 cleavage at G10 indicate reduced dynamics in the lower stem of RRE on complex formation. The marked enhancement of V1 cleavage of the upper stem, specifically G24−C28, suggests that DB340 binding in the internal loop also induces better stacking and/or reduced dynamics in the upper stem and hairpin loop. In contrast, the first base of the loop, A29, and the first base in the duplex at the 3′ side of the hairpin loop, G32, show enhanced cleavage by RNase A and RNase T1, respectively. It is clear that the conformational changes induced in the internal loop by DB340 are propagated into the upper hairpin stem and extend over a long range through the double-helical stack. This agrees with the slight NMR resonance shifts observed for the loop region of RRE. Perhaps the most significant change in RNase cleavage is the protection from V1 cleavage at A50 upon complex formation. As discussed below, NMR results suggest that part of the drug dimer binds at this site.

Imino proton NMR spectra of large RNA systems can provide specific information about the conformation and conformational changes of the RNA upon complex formation (*48*). Imino proton results have shown that RRE undergoes conformational changes in the transition from free RNA to the Rev complex (*37*, *38*). Results with the DB340 complex are similar to those induced by Rev binding. The internal loop region signals become significantly more narrow on addition of DB340, indicating a much more highly structured internal loop in the DB340 complex than in free RRE. The imino NMR results also agree with footprinting results on the DB340 complex indicating that the compound binds in the internal loop region. Binding in the internal loop explains the inhibitory activity of DB340 against Rev/RRE complex formation. A very important feature of the imino proton titration spectra is the observation that at a 1:1 ratio of DB340 to RRE, approximately one-half of the signal intensity of the unbound RRE signals remains, while a new set of imino signals has appeared. At a 2:1 ratio, none of the original signal remains, and the spectrum is dominated by the new set of signals that appeared at the 1:1 ratio. These results demonstrate that a dominate single 2:1 complex of DB340 with RRE forms throughout the titration and that this complex is in slow exchange with free RRE. Some line broadening but no significant further spectral change was observed when additional DB340 (3:1) was added (data not shown). This suggests that above the 2:1 ratio, some weaker nonspecific interactions occur.

Results from the nonexchangeable proton spectral region also support formation of a 2:1 complex. Results from COSY spectra provide clear-cut evidence for a 2:1 complex even at a 1:1 molar ratio. There are 14 pyrimidine bases in the RRE hairpin and 14 COSY cross-peaks for the H5−H6 protons are observed in both the free and the DB340-bound RRE at a 2:1 ratio (data not shown). In contrast, free DB340 has single COSY cross-peaks for the furan aromatic protons, the benzimidazole protons and the phenyl proton pairs, while all of these signals are doubled in the complex of DB340 with RRE at both 1:1 and 2:1 molar ratios. Rotation of the phenyl ring is reduced upon complex formation resulting in separate resonances for the two sets of phenyl ring protons, although only 3 of the 4 sets of resonances are resolved (Figure 4).

Cross-peaks between DB340 and RRE in NOESY spectra of the 2:1 complex place the drug dimer in the minor groove of RRE near the G−A base pair end of the internal loop. Specifically, cross-peaks between the H2 of A28 and both furan protons of one DB340 molecule are observed, orienting the furan moiety toward the RNA bases. A cross-peak to the furan proton b of the second bound DB340 molecule and an unassigned AH2 supports placement of the dimer in the minor groove. Cross-peaks between benzimidazole and furan protons to unassigned H1′ protons further support binding in the minor groove (Figure 5).

The chemical shift changes of the aromatic proton signals of DB340 are all upfield on complex formation. The shifts are 0.6 to 1.1 ppm for the furan, 0.2 to 0.5 ppm for the phenyl groups, and 0.3 to 0.6 for the benzimidazole proton signals. These results strongly suggest that the two bound molecules of DB340 are somewhat stacked on each other in the 2:1 complex with RRE. Although an intercalation complex could also result in upfield shifts of the DB340 aromatic signals, the cross-peaks discussed above place the complex in the minor groove. Additionally, the CD changes of RRE are very small on complex formation with DB340 (as with the Rev complex) and would be much larger if intercalation occurred, and intercalative binding generally does not give the very large equilibrium binding constants and specific binding obtained for the RRE-DB340 complex. The complex also has a very large association rate constant, again suggesting a groove binding mode with no significant base pairing changes in the RNA duplex stems. Although the NMR spectra of the DB340−RRE complex are rather clean considering the complexity of the system, there is too much overlap and ambiguity to enable a detailed solution structure to be obtained with the current system. Solving the solution

structure of this complex will necessitate extensive studies with several specifically labeled RRE samples.

It is initially surprising that a tetracationic molecule with positive charges symmetrically distributed around the furan center of the molecule will dimerize. It is plausible that the highly anionic charge of RNA provides an environment suitable for dimerization. Indeed, the cooperative binding mode of the dimer indicates that dimerization does not precede binding. It is likely that neutralization of the tetracationic charge of the first molecule upon binding to RNA is necessary for dimerization.

DB340 binds to RRE with high affinity, but the tetracationic charge of the molecule facilitates a high degree of nonspecific binding and complicates therapeutic development of the molecule. The discovery of the minor groove dimer complex of DB340 does provide an exciting new model for RNA-directed drug design and furthers our knowledge about the mechanisms and possibilities of drug binding to RNA. Work on a high-resolution structure of the complex and studies with derivatives of DB340 are proceeding.

## REFERENCES


1. Oldstone, M. B. A. (1998) *Viurses, Plagues, and History*, Oxford University Press, Oxford.
2. Sucheck, S. J., Wong, A. L., Koeller, K. M., Boehr, D. D., Draker, K.-A., Sears, P., Wright, G. J., and Wong, C.-H. (2000) *J. Am. Chem. Soc. 122*, 5230−5231.
3. Michael, K., and Tor, Y. (1998) *Chem. Eur. J. 4*, 2091−2098.
4. Wilson, W. D., and Li, K. (2000) *Curr. Med. Chem. 7*, 73−98.
5. Walter, F., Vicens, Q., and Westhof, E. (1999) *Curr. Opin. Chem. Biol. 3*, 694−704.
6. Li, K., Fernandez-Saiz, M., Rigl, C. T., Kumar, A., Ragunathan, K. G., McConnaughie, A. W., Boykin, D. W., Schneider, H. J., and Wilson, W. D. (1997) *Bioorg. Med. Chem. 5*, 1157−1172.
7. Hermann, T., and Westhof, W. (1998) *Curr. Opin. Biotech. 8*, 278−285.
8. Chow, C., and Bogdan, F. M. (1997) *Chem. Rev. 97*, 1489−1513.
9. Afshar, M., Prescott, C. D., and Varani, G. (1999) *Curr. Opin. Biotech. 10*, 59−63.
10. Hermann, T., and Westhof, E. (1999) *J. Med. Chem. 42*, 1250−1261.
11. Wong, C.-H., Hendrix, M., Manning, D. D., Rosenbohm, C., and Greenberg, W. A. (1998) *J. Am. Chem. Soc. 120*, 8319−8327.
12. Wilson, W. D. (1999) in *Comprehensive Natural Products Chemistry* (Kool, E. T., Ed.) pp 427−476, Elsevier Science Ltd., Oxford.
13. Wemmer, D. E., and Dervan, P. B. (1997) *Curr. Opin. Chem. Biol. 3*, 355−361.
14. Wilson, W. D. (1996) in *Nucleic Acids in Chemistry and Biology* (Blackburn, G. M., and Gait, M. J., Eds.) pp 329−374, Oxford University Press, New York.
15. Geierstanger, B. H., and Wemmer, D. E. (1995) *Annu. Rev. Biophys. Biomol. Struct. 24*, 463−493.
16. Bailly, C. (1998) in *Advances in DNA Sequence Specific Agents* (Palumbo, M., Ed.) pp 97−156, JAI Press Inc., Greenwich, CT.
17. Bailly, C., and Chaires, J. B. (1998) *Bioconj. Chem. 9*, 513−538.
18. Dervan, P. B., and Burli, R. W. (1999) *Curr. Opin. Chem. Biol. 6*, 688−693.
19. Wemmer, D. E. (2000) *Annu. Rev. Biophys. Biomol. Struct. 29*, 439−461.
20. Wang, L., Bailly, C., Kumar, A., Ding, D., Bajic, M., Boykin, D. W., and Wilson, W. D. (2000) *Proc. Natl. Acad. Sci. 97*, 12−16.
21. Mazur, S., Tanious, F. A., Ding, D., Kumar, A., Boykin, D. W., Simpson, I. J., Neidle, S., and Wilson, W. D. (2000) *J. Mol. Biol. 300*, 1−17.
22. Niedle, S., Ed. (1999) in *Oxford Handbook of Nucleic Acid Structure*, Oxford University Press, Oxford.
23. Tinoco, I. J., and Bustamanta, C. (1999) *J. Mol. Biol. 293*, 271−281.
24. Wilson, W. D., Tanious, F. A., Buczak, H., Venkatramaman, M. K., Das, B. P., and Boykin, D. W. (1990) (Pullman, B., and Jortner, J., Eds.) pp 331−353, Kluwer Academic Publishers, The Netherlands.
25. Boykin, D. W., Kumar, J., Spychala, J., Zhou, M., Lombardy, R. J., Wilson, J. D., Dykstra, C. C., Jones, S. K., Hall, J. E., Tidwell, R. R., Laughton, C., Nunn, C. M., and Neidle, S. (1995) *J. Med. Chem. 38*, 912−916.
26. Zapp, M. L., Young, D. W., Kumar, A., Singh, R., Boykin, D. W., Wilson, W. D., and Green, M. R. (1997) *Bioorg. Med. Chem. 5*, 1149−1155.
27. Zhao, M., Ratmeyer, L., Peloquin, R., Yao, S., Kumar, A., Spychala, J., Boykin, D. W., and Wilson, W. D. (1995) *Bioorg. Med. Chem. 3*, 785−794.
28. Ratmeyer, L., Zapp, M. L., Green, M. J., Vinayak, R., Kumar, A., Boykin, D. W., and Wilson, W. D. (1996) *Biochemistry 35*, 13689−13696.
29. Li, K., Xiao, G., Rigl, T., Kumar, A., Boykin, D. W., and Wilson, W. D. (1998) in *Structure, Motion, Interaction and Expression of Biological Macromolecules* (Sarma, R. H., and Sarma, M. H., Eds.) pp 137−145, Adenine Press.
30. Calnan, B. J., Tidor, B., Biancalana, J., Hundson, D., and Frankel, A. D. (1991) *Science 252*, 1167−1171.
31. Calnan, B. J., Biancalana, S., Hudson, D., and Frankel, A. D. (1991) *Genes Dev. 5*, 201−210.
32. Rigl, C. T., Lloyd, D. H., Tsou, D. S., Gryaznov, S. M., and Wilson, W. D. (1997) *Biochemistry 36*, 650−659.
33. Heaphy, S., Finch, J. T., Gait, M. J., Karn, J., and Singh, M. (1991) *Proc. Natl. Acad. Sci. U.S.A. 88*, 7366−7370.
34. Peytou, V., Condom, R., Patino, N., Guedj, R., Aubertin, A. M., Gelus, N., Bailly, C., Terreux, R., and Cabrol-Bass, D. (1999) *J. Med. Chem. 42*, 4042−4053.
35. Weeks, K. M., and Crothers, D. M. (1991) *Cell 66*, 577−588.
36. Piotto, M., Saudek, V., and Sklenar, V. (1992) *J. Biomol. NMR 2*, 661−665.
37. Battiste, J. L., Mao, H., Rao, N. S., Tan, R., Muhandiram, D. R., Kay, L. E., Frankel, A. D., and Williamson, J. R. (1996) *Science 273*, 1547−1551.
38. Peterson, R. D., and Feigon, J. (1996) *J. Mol. Biol. 264*, 863−877.
39. Kjems, J. R., Calnan, B. J., Frankel, A. D., and Sharp, P. (1992) *EMBO J. 11*, 1119−1129.
40. Umezawa, H., and Hooper, I. R., Eds. (1982) *Aminoglycoside Antibiotics*, Springer-Verlag, New York, Heidelberg.
41. von Ahsen, U., Davies, J., and Schroeder, J. (1991) *Nature 353*, 368−370.
42. Rogers, J., Chang, A. H., von Ahsen, U., and Schroeder, R. (1996) *J. Mol. Biol. 36*, 916−925.
43. Wang, S., Huber, P. W., Cui, M., Czarnik, A. J., and Mei, H.-Y. (1998) *Biochem. 37*, 5549−5557.
44. Zapp, M. L., Stern, S., and Green, M. R. (1993) *Cell 74*, 969−978.
45. Mei, H.-Y., Galan, A. j., Halim, N. J., Mack, D. P., Moreland, J. W., Sanders, K. B., Truong, H. N., and Czarnik, A. J. (1995) *Bioorg. Med. Chem. Lett. 5*, 2755.
46. Tiley, L. S., Malim, M. H., Tewary, H. K., Stockley, P. G., and Cullen, B. R. (1992) *Proc. Natl. Acad. Sci. U.S.A. 89*, 758.
47. Cook, K. S., Fisk, G. J., Hauber, J., Usman, N., Daly, T. J., and Rusche, J. R. (1991) *Nucleic Acids Res. 19*, 1577.
48. Wu, M., and Tinoco, I. J. (1998) *Proc. Natl. Acad. Sci. U.S.A. 20*, 11555.


BI002338B